

*Invited Paper*

# Three-dimensional helix terahertz metamaterials with mechanical tunability

Yonggang Piao <sup>1†</sup>, Helin Li <sup>1,3†</sup>, Zhongyang Bai <sup>4</sup>, Haowei Sun <sup>3,4</sup>, Xinyu Wu <sup>5</sup>, Tong Sun <sup>1,3</sup>, Yousheng Zhou <sup>1</sup>, Qinghe Ye <sup>1</sup>, Michael Kraft <sup>5</sup>, Xiaojun Wu <sup>4</sup>, Tianxiao Nie <sup>1,2,3</sup>, Weisheng Zhao <sup>1,3</sup> and Lianggong Wen <sup>1\*,2,3</sup>

<sup>1</sup> School of Integrated Circuit Science and Engineering, Beihang University, Beijing, 100191, China.

<sup>2</sup> Beihang Hangzhou Innovation Institute Yuhang, Beihang University, Xixi Octagon City, Yuhang District, Hangzhou, 310023, China.

<sup>3</sup> Beihang-Goertek Joint Microelectronics Institute, Qingdao Research Institute of Beihang University, Qingdao, 266000, China.

<sup>4</sup> School of Electronics and Information Engineering, Beihang University, Beijing 100191, China.

<sup>5</sup> MNS-MICAS, KU Leuven, Leuven-3001, Belgium.

<sup>†</sup> These authors contributed equally to this paper.

\*1 Email: wenlg@buaa.edu.cn

(Received November 18, 2021)

**Abstract:** Terahertz polarization modulation plays a key role in a variety of applications, and terahertz metamaterials composed of artificially designed structures can modulate terahertz waves efficiently. These structures determine the electromagnetic properties of the metamaterial, resulting in effective control of the electromagnetic (EM) effects. Currently, most of the active metamaterial is based on planar unit structures, which can be modulated by using electrical, optical, thermal and magnetic methods. In this paper, a 3D helix metamaterial is proposed, which is fabricated by projection micro stereolithography and atomic layer deposition (ALD). The operation condition modelling proved that the helix metamaterials can transform a THz linear polarization wave to a right-handed circular polarization wave. The experimental result also shows that the polarization rotation angle increases from 14.1° to 26.0° and the ellipticity angle decreases from 23.5° to 9.2° with the pitch of the helical structure varying from 157  $\mu\text{m}$  to 250  $\mu\text{m}$  at 0.27 THz. Furthermore, the maximum range of terahertz circular dichroism varies from -6.0° to 30.0° in the same conditions. By changing the structural parameters mechanically or combining with other adjustable mechanical devices, the metamaterials are expected to enable more extensive applications with EM interference resistance, using merely mechanical control methods.

**Keywords:** Terahertz, 3D helix metamaterial, Projection micro-stereo-lithography, Polarize modulation, Mechanical control

**doi:**

## 1. Introduction

Terahertz (THz) waves, which range from 100 GHz to 10 THz [1-3], represent an interesting research topic due to their unique properties, such as broadband [4], coherence [5], low energy and rich spectral information [6, 7]. Recently, Terahertz technology has been widely utilized for various remarkable applications, benefiting from stable and reliable terahertz emission sources.

As a key component of THz device, Terahertz polarization modulation has numerous applications, such as imaging [8], medical diagnosis and high-speed communication [9-11]. Metamaterials, with the capacity of effectively controlling the electromagnetic (EM) properties of terahertz waves, have been demonstrated as one of the most promising methods of modulating terahertz waves in recent research [12]. Compared with natural materials, metamaterials have unusual physical characteristics, including negative refractive index [13], negative permittivity and negative magnetic permeability [14, 15], which mainly depend on periodic arrangements of sub-wavelength resonant units.

According to the structure of the metamaterials, it can be divided into two-dimensional (2D) and three-dimensional (3D) metamaterials [16, 17]. Recently, it has been demonstrated that 2D-metamaterial-based devices can modulate EM waves by various artificial periodic structures [18, 19], like thin metal wires [14], split resonance rings [15] and net structures [20]. Compared with 3D metamaterials, 2D metamaterials can be relatively simply fabricated in different manufacturing techniques, including MEMS and CMOS technology [21], and they can be integrated with spintronic THz emitters as bio-sensors [22, 23]. A disadvantage of 2D metamaterials is that they do not have chiral optical properties like circular dichroism (CD) and optical activity (OA), which 3D chiral metamaterials have [24]. The chirality means that the structural unit (e.g. a helix) cannot be coincident with its mirror image by translation or rotation transformation [25]. In modern optical systems, chiral materials are widely used to control the polarization of the light wave. Compared with natural chiral materials, 3D chiral metamaterials have better optical chirality because of the artificially periodic structures. 3D chiral metamaterials have wide applications in biological detection, chemical analysis, chiral light detectors and other fields [26-28]. Furthermore, the strong circular polarization selective response also makes 3D chiral metamaterials which plays a key role in spin photonics and optical polarization modulation.

However, the fabrication process is a considerable challenge as it is incompatible with traditional micro-nano process technologies. A 3D helix metamaterial that can work in the infrared band was fabricated by combining femtosecond laser 3D direct writing and electrochemical deposition technology [28]. However, this method cannot be used to fabricate nanostructures operating in the near-infrared and visible wavelengths because of the optical diffraction limit. Focused ion or electron beam induced deposition was used to reduce the size of helix structure, but the chirality was not as expected [29]. Other processing methods such as edge photolithography [30], sweep angle deposition [31] and inclination angle etching [32] were also used to fabricate 3D chiral structures. Additionally, research of the tunability of the 3D chiral metamaterials also has attracted attention recently. An origami-based reconfigurable metamaterial for the microwave band for tunable chirality was proposed by Wang [33], and it can demonstrate multiple functionalities, such as broadband control of the amplitude, polarization and phase of the EM waves by reconstructing the actively modulating the 3D metamaterials with external force. However, the realization of the origami metamaterials in the THz band still faces

considerable challenges.

In this work, a 3D helix metamaterial with mechanical tunability is proposed, which is fabricated by projection micro stereolithography (PμSL). The surface of the metamaterials is made of conductive materials by atomic layer deposition (ALD), therefore, sufficient free electrons inside the helix material can interact with the electromagnetic field in the terahertz band. The device can transform the incident THz linear polarization wave to a right-handed circular polarization (RCP) wave. By controlling the pitch of the helical structure from  $157\ \mu\text{m}$  to  $250\ \mu\text{m}$ , the modulation effect shows the maximum range of TCD varies from  $-6.0^\circ$  to  $30.0^\circ$ . The height change can be achieved by the mechanical modulation method, which extensively avoids electromagnetic interference for a variety of applications. The 3D helix metamaterials have potential for applications in optoelectronic devices, terahertz imaging and signal modulation.

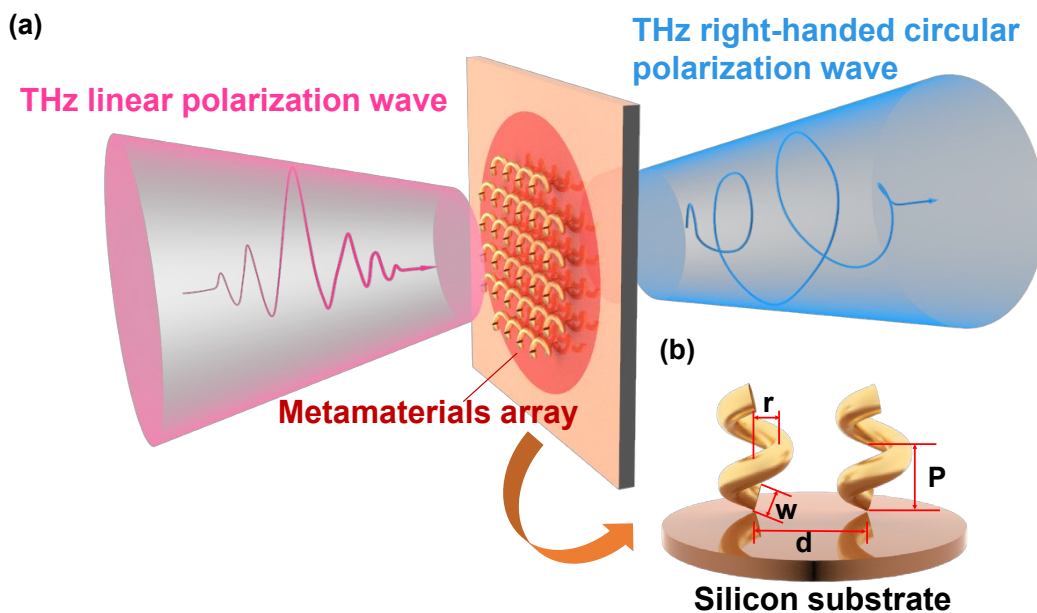


Fig. 1 Illustration of the designed three-dimensional helix terahertz metamaterials. (a) Schematic of the 3D helix terahertz metamaterials with mechanical tunability, it can transform the incident THz linear polarization wave to right-handed circular polarization wave by the metamaterials array; (b) key parameters of the helix metamaterials.

## 2. Materials and methods

### 2.1 Device design

A schematic of the designed helix metamaterials is shown in Fig.1 (a), which illustrates the concept and the main parameters of the device. A micro-structured monomers array is uniformly arranged in a circular area. When stimulated by the linearly polarized incident wave, the emitted wave will become circularly polarized, and the degree of circulation will vary due to the changes

of the pitch ( $P$ ), which corresponds to the height of one complete helix turn. The cross-sectional diameter  $w$  of the helix structure is  $70 \mu\text{m}$  while the wire diameter  $r$  is  $65 \mu\text{m}$ . Considering the feasibility of device fabrication that the turns number  $N$  was set as 1.5. The pitch ( $P$ ) of the helix is 157, 177 and  $250 \mu\text{m}$ , respectively, the height of the device is defined as  $N \cdot P$ , the outer diameter of the 3D helix metamaterial unit is set to be  $200 \mu\text{m}$ , the diameter of 3D helix metamaterial array is  $4 \text{mm}$ , and the distance between the centres of two adjacent structures  $d$  is  $300 \mu\text{m}$ . In order to interact with the electromagnetic field in the terahertz band,  $50 \text{nm}$  AZO (aluminium doped zinc oxide) film is deposited on the structures to facilitate sufficient free electrons while the helix metamaterials are stimulated. The structural parameters of the device are shown in Fig.1 (b). The designed structure realizes efficient incident wave transmission and polarization conversion.

## 2.2 Operation condition modelling

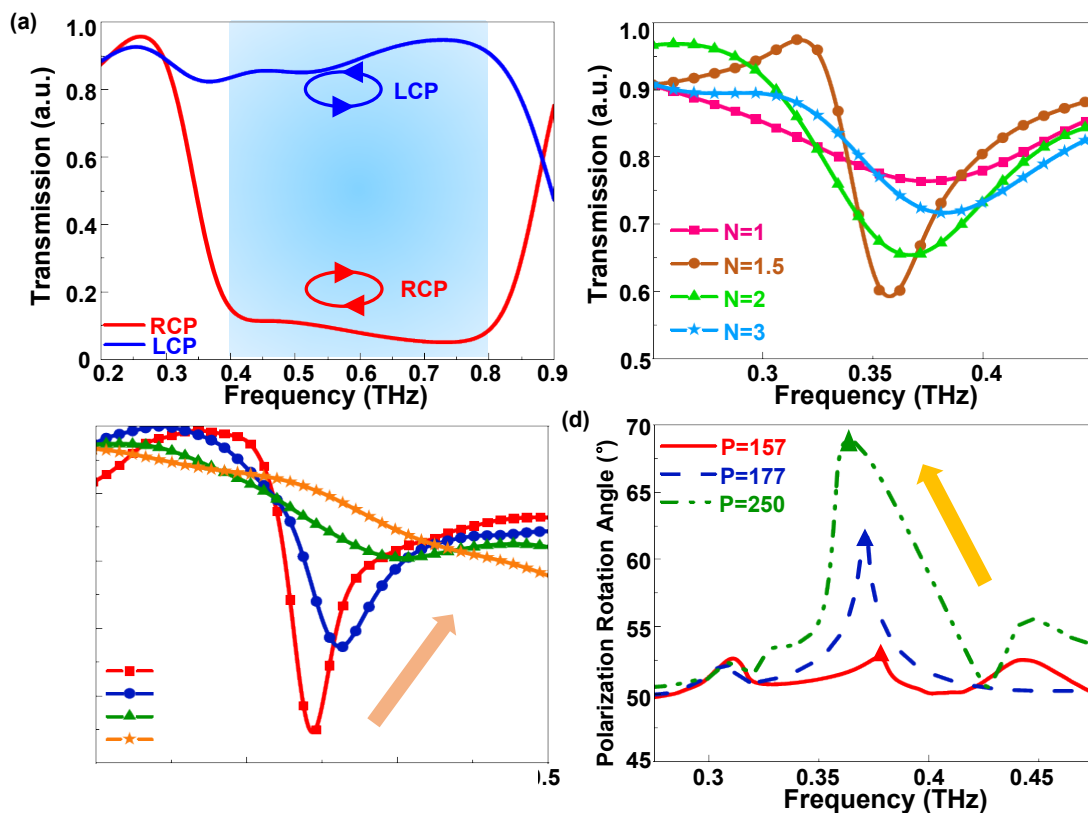


Fig. 2 The modelling of the device in different operation conditions. (a) Comparison of the transmission when the signals are RCP and LCP; (b) change of the transmission with various turn number of the helix structure  $N$ ; (c) influence of the  $P$  on transmission from 157 to  $300 \mu\text{m}$  when  $N=1.5$ ; (d) difference of the polarization rotation angle when changing the  $P$  from 157 to  $250 \mu\text{m}$ .

Finite element modelling software (COMSOL Multiphysics) solves the electric field component in space at a given point in time, after a finite number of cycles, thus the transient and steady-state characteristics of the space electromagnetic field can be obtained [34]. The default

settings of the modelling are: xy direction is the periodic boundary, z-direction is the boundary of the perfect matching coefficient layer, and the bottom is set as a silicon substrate. The transmittance of the periodic nanostructure for the normal incident wave (incident from the air medium) is modelled with a single unit cell with periodic boundary conditions. In order to ensure that the device has polarization modulation capability, left-hand circular polarization (LCP) and right-hand circular polarization (RCP) incident wave is respectively applied to the system, which is synthesized by two linearly polarized waves with a phase difference of  $90^\circ$  in the x and y direction, and a wave incident along the z-axis. The simulation frequency band ranges from 0.1 to 1 THz. Fig.2 (a) shows the differences between the absorption of LCP and RCP waves. As shown in the figure, the LCP basically transmits at 0.4-0.8 THz and the average transmission is 80%; for RCP, the average transmission in the same frequency range but is maintained at 10%, indicating a clear stop band. From the angle of the antenna acceptance, the metal microstructure and the incident wave are right-handed, mutual coupling produces induced current and most of the energy of the incident is absorbed [35].

To analyze the effect of the device on the linearly polarized incident wave, firstly, the transmission diagrams with different turns  $N$  of the helix metamaterials were modelled and the results are presented in Fig.2 (b). When  $N = 1$ , a resonance phenomenon is not observed, while there is an obvious minimum in the transmission for  $N = 1.5$  at 0.35 THz. For  $N > 1.5$  the resonance point is visible but is not stronger, indicating that the resonant frequency is not proportional to the equivalent total length of the helix wire. In order to observe the transmission spectrum and quantitatively analyse the shift of the resonance point,  $N = 1.5$  is used in the following. Fig.2 (c) illustrates the transmission with the  $P$  adjusts from 157 to 250  $\mu\text{m}$ . As shown in the fig.2 (c) the resonance point changes from 0.343 to 0.371 THz, every time  $P$  increases by 50  $\mu\text{m}$  on average and the resonance point shifts by 0.01 THz, while the peak transmission changes from 0.431 to 0.773. When  $P$  increases to 350  $\mu\text{m}$ , the resonance peak disappears, which indicates that the helix structure loses its tuning function when  $P$  is too large. As shown in Fig.2 (d), the polarization rotation angle varies from  $47.7^\circ$  to  $63.8^\circ$  with  $P$  ranging from 157 to 250  $\mu\text{m}$  around 0.37 THz, which demonstrates that the device has an effective polarization modulation capability.

### 2.3 Device fabrication and experimental setup

For fabrication of the nanostructure P $\mu$ SL was used, which is mainly employed to make soft materials such as hydrogels and polymers with Stereolithography (3D printing) [36]. The P $\mu$ SL uses a high-precision ultraviolet lithography projection system to project the pattern to be printed onto the liquid surface of the resin, allowing to realise complex 3D shapes from a digital model. We fabricated several sets of 3D helix structure arrays with different heights using high-precision hard resins, GR resin (Boston Micro Fabrication, China). Under 0.45Mpa, the thermal deformation temperature of this material is 102°C, which fulfils the thermal requirements for the metallization of the structures. The designed pattern of the 3D helix metamaterials was modelled layer by layer. After that, the devices were fabricated according to the following processing steps.

First, each pattern layer was transferred to the negative photosensitive resin under UV lithography, as shown in Fig.3 (a). Subsequently, the 3D helix metamaterials were developed and cured. The cycle was repeated until each layer was superimposed to form the final structure (Fig.3 (b)). Finally, the metallization was completed by using atomic layer deposition (ALD), with which 50 nm AZO was deposited, as depicted in Fig.3 (c). Fig.3 (d)-(f) show SEM images focused on different details of the metamaterials array and the nanostructured unit.

THz emission experiments were conducted using a THz time-domain spectrometer (THz-TDS) system with a linear polarization source [28], as shown in Fig.4. The average output power of femtosecond laser was 1.18 W, and the sapphire laser oscillator had a pulse duration of 70 fs and repetition rate of 80 MHz, with a central wavelength of 800 nm. The laser beam was divided into two parts by a non-polarizing beam splitter (10:1), where the more powerful beam was used for stimulating the device, whereas the residual beam was collinearly focused with the THz signal as the probe wave onto the ZnTe crystal for signal detection. All measurements were conducted in a vacuum chamber to avoid the influence of moisture.

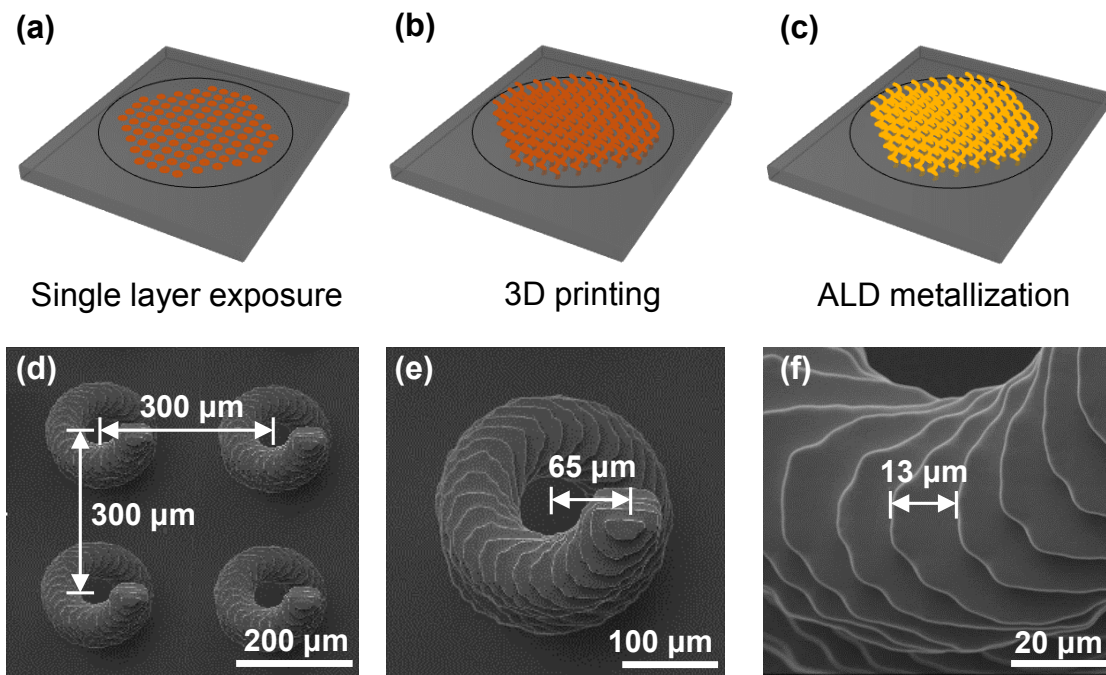


Fig. 3 Demonstration of the fabrication processing and the SEM micrographs. (a) Stratifying and exposing a single layer; (b) Repeating the printing process to form the final 3D structure and (c) Metallizing the surfaces of the metamaterials array by ALD; (d)-(f) The SEM micrographs and the critical dimensions of the helix metamaterials array.

As illustrated in Fig.4, the generated terahertz polarization was vertical to the optical table (defined as the y-axis). To measure the polarization of the electric field components  $E_x$  and  $E_y$  through the device, the first polarizer (P1) was placed in front of the source to ensure a pure and stable polarization of incident. Its transmission direction was the y-axis. The second polarizer (P2) was placed behind the device and installed on an electric rotating table controlled by a computer,

which projected the transmitted wave to the polarization direction to be measured. Before the transmission signal passed through the detection crystal, the polarizer (P3) was fixed to project the electric fields of different directions to the y-axis for measurement. Since the helix structure was not symmetrical, it was necessary to measure the two vertical polarizations (horizontal and vertically polarized THz waves) incident on the metamaterials to characterize the in-plane optical properties of the device, which was accomplished by rotating the device by  $90^\circ$  instead of rotating the THz emitter. The wave without passing the device was used as the reference for the measurement. There were two possible configurations for the measurements: the device may be mounted horizontally (HD) or vertically (VD) relative to the input linear polarization.

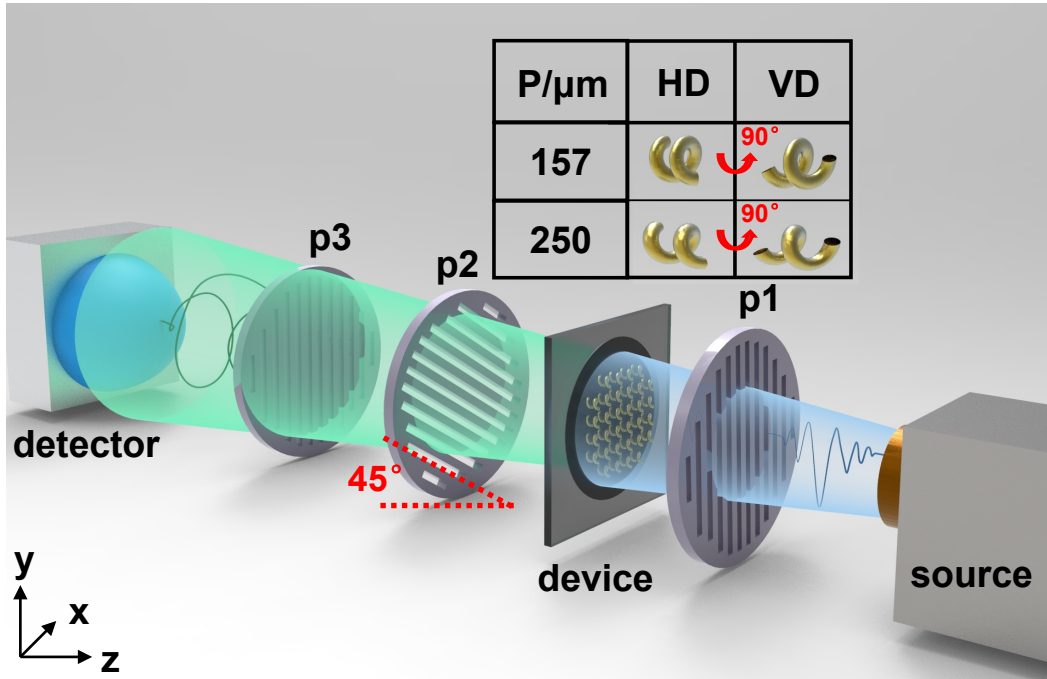


Fig. 4 Schematic diagram of the THz domain system in this work.

### 3. Results and discussion

As mentioned above, the x and y-components of the electric field can be calculated by Eq. (1):

$$E_{x/y}(t) = E_{+45^\circ}(t) \mp E_{-45^\circ}(t), \quad (1)$$

where  $E_{+45^\circ}(t)$  and  $E_{-45^\circ}(t)$  are the time-domain electric field measurements when the transmission orientation of polarizer P2 are at  $+45^\circ$  and  $-45^\circ$  relative to that of the polarizer P1, respectively.

The complex frequency-domain electric field spectra ( $\tilde{E}_{x/y}$ ) were obtained using fast Fourier transform (FFT). The Jones transfer matrix of a sample can be defined as  $T$ .

When the device is installed horizontally, the electric field vector of the transmitted THz wave through the device  $\tilde{E}_s$  is related to the incident electric field  $\tilde{E}_{in}$  by  $\tilde{E}_s = T\tilde{E}_{in}$ , where  $\tilde{E}_{in}$  is the reference signal measured by the system without the device. In the measurement, it is always along the y-direction. After rotating the device by  $90^\circ$  as vertical orientation, the measured transmitted signal is related to the reference signal as depicted in Eq. (2):

$$\tilde{E}_s^v = R(90^\circ)TR(-90^\circ)\tilde{E}_{in}. \quad (2)$$

In Eq. (2), superscripts indicate the abbreviation of mounting orientation, where  $R(\theta)$  is the rotation matrix with rotation angle  $\theta$ :

$$R(\theta) = \begin{pmatrix} \cos(\theta) & -\sin(\theta) \\ \sin(\theta) & \cos(\theta) \end{pmatrix}. \quad (3)$$

By calculating  $R(\theta)$ , the Jones transfer matrix  $T$  of the device can be obtained. Since the polarization of the incident THz beam is linear and vertical, the polarization rotation angle  $\beta$  and the ellipticity angle  $\eta$  caused by the device can be calculated by the Stokes parameter directly [35], and the same equation can be applied to the horizontal and vertical directions of the installation. The four Stokes parameters are defined by:

$$\begin{pmatrix} S_0 \\ S_1 \\ S_2 \\ S_3 \end{pmatrix} = \begin{pmatrix} \tilde{E}_x^* & \tilde{E}_y^* \\ \tilde{E}_x^* & -\tilde{E}_y^* \\ \tilde{E}_y^* & \tilde{E}_x^* \\ i\tilde{E}_y^* & -i\tilde{E}_x^* \end{pmatrix} \begin{pmatrix} \tilde{E}_x \\ \tilde{E}_y \end{pmatrix}. \quad (4)$$

The polarization rotation angle  $\beta$  relative to the horizontal direction and the ellipticity  $\eta$  can be calculated using the Stokes parameters as:

$$\beta = \frac{1}{2} \tan^{-1} \left( \frac{S_2}{S_1} \right). \quad (5)$$

$$\eta = \frac{1}{2} \sin^{-1} \left( \frac{S_3}{S_0} \right). \quad (6)$$

The Jones matrix elements measured by the linearly polarized incident signal are used to infer the transmitted signal of the circularly polarized incident beam, which pass through the helix device. For normalized right circular polarization (RCP) incident beam  $\tilde{E}_{RCP}^{in}$  [35], the electric field of the transmitted wave is

$$\tilde{E}_{RCP}^{out} = T\tilde{E}_{RCP}^{in}. \quad (7)$$

Similarly, for a normalized left circularly polarized (LCP) incident beam, the magnitude is  $E_{LM}$  and the magnitude of this complex electric field vector is  $E_{RM}$ , representing terahertz circular dichroism (TCD) which is a commonly used quantity to characterize the optical rotation of chiral materials [35]. It is related to the relative transmission (or absorption) difference between the incident waves of RCP and LCP, which can be defined and quantified by [35]:

$$TCD = \tan^{-1} \left( \frac{E_{RM} - E_{LM}}{E_{RM} + E_{LM}} \right). \quad (8)$$

When a linearly polarized (along y-axis) light incident to the device, the polarization angle and ellipticity angle will rotate due to the coupling between the EM wave and the metamaterials. The changes of the polarization rotation angle (PRA) and ellipticity angle (EA) with height are shown in Fig. 5 (a) and (b). The experimental results indicate that the PRA increases from  $14.1^\circ$  to  $26.0^\circ$  and the EA decreases from  $23.5^\circ$  to  $9.2^\circ$  with the pitch of the helical structure varying from 157 to  $250 \mu\text{m}$  at  $0.27 \text{ THz}$ . Normally, the polarization direction of the radiation source before special treatment is usually scattered in various directions. After being polarized by a polarizer, the THz wave will become a wave with a single polarization.

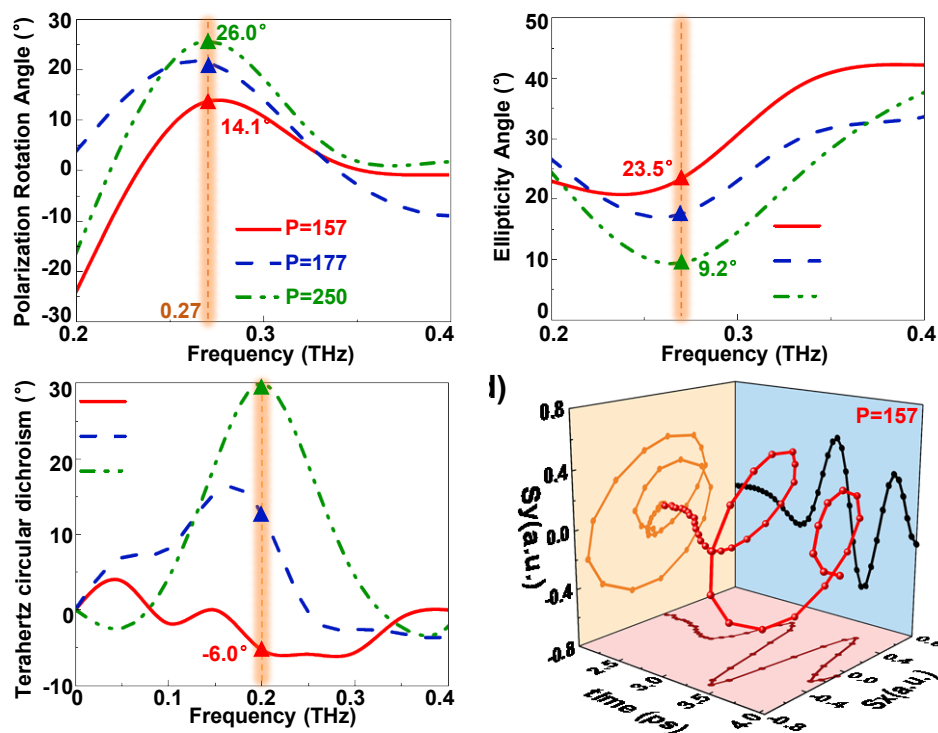


Fig. 5 (a)-(c) Changes of the polarization rotation, ellipticity angle and THz circular dichroism by controlling the P from 157 to  $250 \mu\text{m}$ , respectively; (d) right-handed circular polarized terahertz wave generated by linearly polarized terahertz wave.

When the plane-polarized light passes through the symmetrical molecular structure, it will be divided into two circularly polarized lights, left-handed and right-handed, and finally it will pass through a polarizer to superimpose it into a linearly polarized light. Due to the influence of the helical structures, the left-handed and right-handed circularly polarized light have a difference in refractive index. Therefore, an additional phase difference will be generated after the overlap, and the emitted synthetic linearly polarized light will be deflected in angle. What is produced after superposition is no longer linearly polarized light, but elliptically polarized. Fig.5 (c) shows that the maximum range of TCD varies from  $-6.0^\circ$  to  $30.0^\circ$  with the P varying from 157 to  $250 \mu\text{m}$  in

the vicinity of 0.2 THz. The electric field distribution diagram of one of the devices ( $P=157 \mu\text{m}$ ) in the time domain is shown in Fig.5 (d), which exhibits an obvious right-handed circular polarization of the transmission signal.

The experimental results illustrate that the helix metamaterials have a certain modulating effect on the linearly polarized incident signal, and the effectiveness of the modulation can be adjusted merely by changing the device height, which leads to an extensive range of potential applications such as mechanically modulated terahertz polarizers, meta-surfaces, sensors and other related devices.

#### 4. Conclusions

In conclusion, a helix microstructure was proposed, fabricated by a P $\mu$ SL process and coated with 50 nm AZO film by ALD. The theoretical modelling demonstrated that this nanostructure had an obvious selective effect on circularly polarized incidence. A pass band for LCP and a stop band for RCP from 0.35 THz to 0.8 THz were observed. Moreover, modelling and experiments were performed on linearly polarized incident light. The experiment showed that the modulation effect of the devices on the incident light can be changed by adjusting the P value of the helix structures. The modulation characteristics of the devices with different P were tested. While P varied from 157 to 250  $\mu\text{m}$ , the maximum adjustment ranges of the PRA and EA were 11.9° and 14.3°, respectively, at 0.27 THz. Moreover, the TCD modulation angle range of the devices was higher than 30°. The results enrich the approaches to modulate terahertz signals mechanically without EM interference and pave the way to potential terahertz modulation applications.

#### Acknowledgments

This work was supported by the Beihang Hangzhou Innovation Institute Yuhang, Beihang University, “Zhuoyue Program of Associate Professors” of Beihang University (ZG216S18B5), the National Key R&D Program of China (2018YFB0407602) and the National Natural Science Foundation of China (61774013 and 11644004). The authors also would like to thank Institute of Physics, Chinese Academy of Sciences, Hangzhou Innovation Institute, Beihang University and Research Institute of Beihang University in Shenzhen for the assistance in this study.

#### References

- [1] Keren-Zur, S. , et al. "Generation of spatiotemporally tailored terahertz wavepackets by nonlinear metasurfaces". *Nature Communications* 10.1(2019).
- [2] Pawar, Ashish Y., et al. "Terahertz technology and its applications". *Drug invention today* 5,157-163 (2013).

- [3] Serita, Kazunori, et al. "Invited Article: Terahertz microfluidic chips sensitivity-enhanced with a few arrays of meta-atoms". *Apl Photonics* 3,051603 (2018).
- [4] Pavlov, S. G., et al. "Terahertz transient stimulated emission from doped silicon". *APL Photonics* 5,106102 (2020).
- [5] Nishida, Yousuke, et al. "Terahertz coherent receiver using a single resonant tunnelling diode". *Scientific reports* 9,1-9 (2019).
- [6] Herrmann, Eric, et al. "Modulators for mid-infrared and terahertz light". *Journal of Applied Physics* 128,140903 (2020).
- [7] Woodward, Ruth M., et al. "Terahertz pulse imaging in reflection geometry of skin tissue using time-domain analysis techniques". *Clinical Diagnostic Systems: Technologies and Instrumentation*. Vol. 4625. International Society for Optics and Photonics (2002).
- [8] Ojefors, Erik, et al. "A 0.65 THz focal-plane array in a quarter-micron CMOS process technology". *IEEE Journal of Solid-State Circuits* 44,1968-1976 (2009).
- [9] Serita, Kazunori, et al. "Invited Article: Terahertz microfluidic chips sensitivity-enhanced with a few arrays of meta-atoms". *Apl Photonics* 3,051603 (2018).
- [10] Tonouchi, Masayoshi. "Cutting-edge terahertz technology". *Nature photonics* 1,97-105 (2007).
- [11] Kleine-Ostmann, Thomas, and Tadao Nagatsuma. "A review on terahertz communications research". *Journal of Infrared, Millimeter, and Terahertz Waves* 32,143-171 (2011).
- [12] Ding, Fei, Anders Pors, and Sergey I. Bozhevolnyi. "Gradient metasurfaces: a review of fundamentals and applications". *Reports on Progress in Physics* 81, 026401 (2017).
- [13] Smith, David R., et al. "Composite medium with simultaneously negative permeability and permittivity". *Physical review letters* 84,4184 (2000).
- [14] Pendry, John B., et al. "Extremely low frequency plasmons in metallic mesostructures". *Physical review letters* 76 ,4773 (1996).
- [15] Pendry, John B., et al. "Magnetism from conductors and enhanced nonlinear phenomena". *IEEE transactions on microwave theory and techniques* 47,2075-2084 (1999).
- [16] Chen, Menglin LN, Li Jun Jiang, and Wei EI Sha. "Artificial perfect electric conductor-perfect magnetic conductor anisotropic metasurface for generating orbital angular momentum of microwave with nearly perfect conversion efficiency". *Journal of Applied Physics* 119,064506 (2016).
- [17] Kaelberer, T., et al. "Toroidal dipolar response in a metamaterial". *Science* 330,1510-1512 (2010).
- [18] Mohammadi Shirkolaei, Morteza, and Javad Ghalibafan. "Unbalanced CRLH behavior of ferrite-loaded waveguide operated below cutoff frequency". *Waves in Random and Complex Media*, 1-16 (2020).
- [19] Alibakhshikenari, Mohammad, et al. "A comprehensive survey of "metamaterial transmission-line based antennas: design, challenges, and applications"". *IEEE Access* 8,144778-144808 (2020).
- [20] Dolling, Gunnar, et al. "Low-loss negative-index metamaterial at telecommunication wavelengths". *Optics letters* 31,1800-1802 (2006).

- [21] Liu, Yongshan, et al. "Active tunable THz metamaterial array implemented in CMOS technology". *Journal of Physics D: Applied Physics* 54,085107 (2020).
- [22] Bai, Zhongyang, et al. "Near-field terahertz sensing of HeLa cells and Pseudomonas based on monolithic integrated metamaterials with a spintronic terahertz emitter". *ACS Applied Materials & Interfaces* 12, 35895-35902 (2020).
- [23] Liu, Yongshan, et al. "Generation of tailored terahertz waves from monolithic integrated metamaterials onto spintronic terahertz emitters". *Nanotechnology* 32,105201(2020).
- [24] Wu, Lin, et al. "Circular polarization converters based on bi-layered asymmetrical split ring metamaterials". *Applied Physics A* 116,643-648 (2014).
- [25] Zhao, R., et al. "Conjugated gammadion chiral metamaterial with uniaxial optical activity and negative refractive index". *Physical Review B* 83,035105 (2011).
- [26] Hendry, Euan, et al. "Ultrasensitive detection and characterization of biomolecules using superchiral fields". *Nature nanotechnology* 5,783-787 (2010)
- [27] Li, Wei, et al. "Circularly polarized light detection with hot electrons in chiral plasmonic metamaterials". *Nature communications* 6,1-7 (2015).
- [28] Gansel, Justyna K., et al. "Gold helix photonic metamaterial as broadband circular polarizer". *Science* 325,1513-1515 (2009).
- [29] Esposito, Marco, et al. "Nanoscale 3D chiral plasmonic helices with circular dichroism at visible frequencies". *Acs Photonics* 2,105-114 (2015).
- [30] Dietrich, Kay, et al. "Circular dichroism from chiral nanomaterial fabricated by on - edge lithography". *Advanced Materials* 24, OP321-OP325 (2012).
- [31] Mark, Andrew G., et al. "Hybrid nanocolloids with programmed three-dimensional shape and material composition". *Nature materials* 12,802-807 (2013).
- [32] Chen, Yang, Jie Gao, and Xiaodong Yang. "Chiral metamaterials of plasmonic slanted nanoapertures with symmetry breaking". *Nano letters* 18,520-527 (2018).
- [33] Wang, Zuojia, et al. "Origami - based reconfigurable metamaterials for tunable chirality". *Advanced materials* 29,1700412 (2017).
- [34] Wang, Maoyan, et al. "Propagation properties of terahertz waves in a time-varying dusty plasma slab using FDTD". *IEEE transactions on plasma science* 43,4182-4186 (2015).
- [35] Choi, Won Jin, et al. "Terahertz circular dichroism spectroscopy of biomaterials enabled by kirigami polarization modulators". *Nature materials* 18,820-826 (2019).
- [36] Sun, C., et al. "Projection micro-stereolithography using digital micro-mirror dynamic mask". *Sensors and Actuators A: Physical* 121,113-120 (2005).